Journal of Materials Chemistry A

Hierarchical structural designs of ion exchange membranes for flow batteries

Journal:	*Journal of Materials Chemistry A*
Manuscript ID	TA-ART-12-2018-011974.R1
Article Type:	Paper
Date Submitted by the Author:	18-Jan-2019
Complete List of Authors:	Yue, Xiujun; University of California, San Diego, Department of Nanoengineering He, Qian; University of California, San Diego, Department of Nanoengineering Lim, Hee-Dae; University of California, San Diego, Department of Nanoengineering liu, ping; University of California, San Diego, Department of Nanoengineering

Journal Name

ARTICLE

Hierarchical structural designs of ion exchange membranes for flow batteries

Xiujun Yue, [a] Qian He, [a] Hee-Dae Lim, [a] and Ping Liu *[a]

Received 00th January 20xx,
Accepted 00th January 20xx

DOI: 10.1039/x0xx00000x

www.rsc.org/

Membranes for flow batteries need to have both high ionic conductivity and selectivity. The selectivity is particularly important for systems involving two different species such as Fe/Cr since any crossover is irreversible. However, most membranes suffer from a trade-off between the two properties. We address this issue by fabricating a composite cation exchange membrane with a hierarchical structure to ensure mechanical stability, conductivity and selectivity. The membrane features a dense, crack-free tungsten oxide coating layer on Nafion that also penetrates into the Nafion's hydrophilic, ionic cluster regions. Oxide inside the polymer was synthesized *in-situ* in the hydrophilic regions, while a sol-gel method was used to coat the oxide on polymer. The oxide inside the Nafion reduces water uptake and swelling ratio, which is essential to ensure the adhesion of the top oxide layer with Nafion. The top dense oxide layer serves as a highly selective membrane for the cation transport. Maintaining comparable conductivity, the membrane shows that permeability for Fe(II) and Cr(III) ions are decreased by an order of magnitude as compared to Nafion, from 2.66×10^{-7} cm^2 s^{-1} and 8.84×10^{-8} cm^2 s^{-1} to 2.31×10^{-8} cm^2 s^{-1} and 8.34×10^{-9} cm^2 s^{-1} respectively. Noticeably, the oxide coating layer shows three orders of magnitude lower permeability than Nafion. When applied in a lab-scale Fe/Cr flow battery, the cycling stability is significantly improved due to the much reduced crossover. This new membrane design can be extended to other polymer membranes and holds promise for applications in a variety of flow batteries.

Introduction

Utilization of renewable resources, such as wind, solar and tide, has been growing rapidly. This growth is driven by the increasing energy demand and concerns of carbon emission,[1-4] however, large-scale energy storage solutions are required due to the intermittent nature of renewable resources.[5,6] Redox flow batteries (RFB) are one of the promising candidates due to their low cost, long life, rapid response, high mobility and flexibility.[5-13] RFBs store energy in two solutions with different redox couples. The positive and negative electrodes are separated by a selective ion exchange membrane (IEM), which prevents mixing of active species. Most of the leading flow batteries with chemistries such as all-vanadium, all-iron, iron-chromium etc., utilize cation exchange membranes (CEM).[2,5,9-15] Anion exchange membranes (AEM) also have been used, especially for lowering crossover when cations serve as active species.[3,9,10,14,15]

Perfluorinated polysulfonic acid (PFSA) membranes such as Nafion are the most widely used CEMs in RFBs due to their high conductivity and good chemical and thermal stabilities.[10,14-16] However, Nafion membranes suffer from the crossover of active species leading to severe self-discharge and decreased energy efficiency.[2,7,17-19] Various strategies have been proposed to fabricate new composite membranes with reduced crossover.[20] Physical blending with inorganic particles,[21-24] nanotubes,[25,26] graphene,[27-29] metal-organic frameworks (MOFs) and polymers has been extensively studied.[30-33] The crossover rate is reduced by these added materials via reducing the mobile water transportation and the corresponding leakage of hydrated redox active ions.[14] Besides the simple mixing method, fillers such as SiO_2 and TiO_2 could also be synthesized during the membrane formation process via a sol-gel method to achieve uniform distribution.[34-37] In the "infiltration method", fillers are formed in-situ by infiltrating precursors into an existing polymer membrane, resulting in well-dispersed and extremely small particles inside the hydrophilic ionic cluster regions of phase-segregated polymer membranes.[20,38-40] Reduced crossover rates are achieved by the decreased size of the ionic cluster regions. Surface modification, mostly with organic coatings serving as a highly selective layer, has been used to reduce the crossover of active species as well.[41-44]

Inorganic ion conductors are ideal candidates to serve as ion exchange membranes. While perfect selectivity is theoretically possible, most of these conductors tend to be brittle and difficult to handle and use. This difficulty can be circumvented by supporting thin films of ion conductors on porous polymer substrates. Unfortunately, a bilayer inorganic-polymer structu-

[a] Department of Nanoengineering, University of California San Diego, La Jolla, CA 92093, USA. *E-mail: piliu@eng.ucsd.edu
Electronic Supplementary Information (ESI) available. See DOI: 10.1039/x0xx00000x

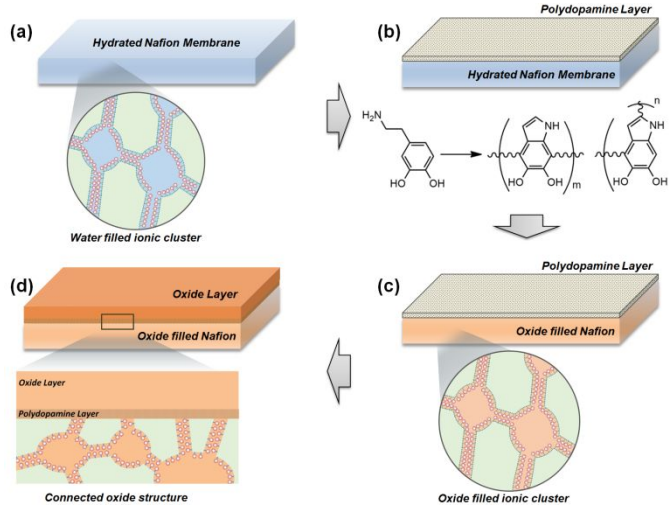

Fig. 1 Fabrication of tungsten oxide/Nafion hierarchical composite membrane (h-DNf/oxide): (a) blank hydrated Nafion membrane; (b) polydopamine coating (DNf); (c) in-situ formation of tungsten oxide in hydrophilic ionic cluster regions of Nafion membrane (c-DNf/oxide); (d) tungsten oxide coating on the surface (h-DNf/oxide). Green: fluorocarbon backbones of Nafion; red spheres: sulfonic acid groups of Nafion.

re has not been widely adopted due to difficulties in integrating materials with significant differences in mechanical properties. Upon exposure to liquids, the polymer tends to swell while the inorganic layer does not. This mismatch results in cracking, delamination and failure of the membrane.

Here, we develop a composite cation exchange membrane with a hierarchical structure, which consists of a polymer membrane with tungsten oxide filling the ionic cluster region and a dense tungsten oxide coating layer on the polymer surface (Fig. 1). This hierarchical structure simultaneously enables both high selectivity and conductivity during use in a flow battery. Tungsten oxide hydrates (H_xWO_3-yH_2O) have been reported to show high proton conductivity (~0.1 S/cm, 25 °C) and are formed in-situ in the ionic clusters of polymer membrane.[45-47] Replacing the water in ionic clusters with oxide achieves several advantages: (1) Decreasing permeability of active species: crossover of active species, such as Fe, Cr, and V ions, primarily relies on hydrated ionic clusters, which cannot permeate through the oxide structure. (2) Enhancing mechanical stability of the membrane: interactions between filled oxide and polymer chains result in denser polymer packing and structural reinforcement. (3) Suppressing swelling of the polymer membrane via the interaction between oxide and polymer chain and decreased water uptake. A low swelling ratio is essential for the polymer membrane to be integrated with a rigid oxide coating layer without the issue of delamination and cracking. The dense oxide layer is coated via a sol-gel method on the polymer/oxide composite membrane. Tungsten oxide hydrates have been reported to have a layered structure with water molecules bonded between the layers which enable efficient proton conduction though the hydrogen bond network.[48] Proton insertion/extraction reactions, $WO_3 + xH^+ + xe^- \leftrightarrow H_xWO_3$, converts tungsten oxide into tungsten bronze (H_xWO_3, $0 < x < 1$). Protons conduct through the movement of proton vacancies.[49] Potassium ions are conducted through a similar solid state ion conduction mechanism. However, multivalent ions, such as Fe, Cr, and V, with high charge density have strong interaction with water molecules which make them too bulky to insert into the lattice structure of tungsten oxide hydrates. Nafion was used as a test case for the hierarchical structure and future experiments can allow for further application of this strategy to other polymer membranes with lower cost. Combining the oxide-in-polymer and oxide-on-polymer structure has great potential to enhance the performance of a variety of membranes.

Experimental

Materials

Nafion 117 membrane was purchased from FuelCellStore. Tungsten powder (12 µm, 99.9% trace metals basis) and Bismuth oxide (Bi_2O_3, 10 µm, 99.9% trace metals basis) was purchased from Sigma-Aldrich. 3-Hydroxytyramine Hydrochloride (dopamine, 99%) was purchased from ACROS Organics. Tris(hydroxymethyl)aminomethane (Tris, 99.8%), hydrogen peroxide solution (H_2O_2, 30%), sulfuric acid (H_2SO_4, 95-98%), hydrochloric acid (HCl, 36.5-38%), potassium chloride (KCl, 99%), ferrous chloride tetrahydrate ($FeCl_2 \cdot 4H_2O$, 99%) and chromium chloride hexahydrate ($CrCl_3 \cdot 6H_2O$, 98%) were purchased from Fisher Scientific.

Membrane preparation

Polydopamine was coated onto Nafion 117 membrane according to literature.[50] Commercial Nafion 117 membrane was pre-treated by boiling in steps of deionized water, starting from pure to a mixture of 3% H_2O_2, and then 0.5 M H_2SO_4 solutions before being stored in deionized water at room temperature. The membrane was then immersed in a 79 ml Tris-HCl buffer (pH 8.5) while 1 ml 160 mg/ml aqueous dopamine solution was added drop wise under mild stirring to induce spontaneous self-polymerization. The coated Nafion membrane (DNf) was taken out after 90 minutes and rinsed with deionized water.

A tungstic acid solution was prepared by slowly dissolving 2.5g tungsten powder in 30 mL 30% hydrogen peroxide in a room-temperature water bath while being stirred. The excess of hydrogen peroxide was removed by placing a small piece of platinum foil in the solution and putting the solution in an oven at 80 °C for 20 minutes. The clear solution turned into bright yellow color.

DNf was soaked in methanol for 24 hours under room temperature and followed by soaking in tungstic acid solution for another 24 hours. Then membrane was wiped residues off and cured for 1 hour under 100% RH and 80 °C environment which was created by placing a capped bottle with water in an oven. All above processes were repeated 3 times to get c-DNf/oxide.

c-DNf/oxide was manually dip coated in the tungstic acid solution resulting in double-sided coatings. The coated Nafion was cured in the same way as the previous method. The coating

and curing steps were repeated three times to achieve h-DNf/oxide with the desired thickness of coating.

Membrane Characterization

The morphology and thickness of h-DNf/oxide was characterized using scanning electron microscopy (FEI Quanta 250 SEM and Zeiss Sigma 500 SEM for ultra-high magnification image) with atomic composition and elemental mapping analysis by an integrated energy-dispersive X-ray (EDX) spectrometer. The chemical composition of the membrane was characterized by Fourier transform infrared spectroscopy (FTIR, Perkin Elmer Spectrum Two) and Raman spectroscopy (Renishaw inVia). The crystal structure of the membrane was investigated by X-ray diffraction (XRD, Brucker D2 Phaser). The thermal stability of membrane was characterized by thermal gravimetric analysis (TGA, Perkin Elmer Pyris 1 TGA) from 25 to 650 °C (heating rate: 5 °C min^{-1}).

Mechanical properties

Mechanical properties of membranes were measured using tensile tests (Instron 5960) to generate stress–strain curves at a strain rate of 0.01 mm s^{-1} at room temperature and sampled at 10 Hz rate. Membrane samples were cut into dog-bone shaped specimen, overall dimensions: 25 mm x 15 mm, gauge dimensions: 15 mm x 2 mm. Dry and wet membranes were pre-treated with mentioned methods for water uptake measurement.

Water uptake and swelling

Water uptake (WU) and in plane area swelling (SW) of membranes were calculated based on the percent change of wet and dry weights (WU) and areas (SW). All measurements were carried out right after treatment for accurate data. Dry membranes were dried at 80 °C under vacuum for 24 hours to remove residual water and then cooled to room temperature under vacuum. Wet membranes were immersed in deionized water at 60 °C for 24 hours to reach complete hydration.

Conductivity

The proton and potassium ion conductivity of the membrane was measured in a conductivity cell using AC impedance spectroscopy and the membrane resistance was probed with a potentiostat (Bio-logic, VSP-300) with an oscillating voltage of 20 mV over a frequency range of 7 MHz–1 Hz. Prior to testing, the membrane sample was fully hydrated in water. The conductivity (σ) was calculated with the following equation:

$$\sigma[\mathrm{mS}\ cm^{-1}] = \frac{L}{RS}$$

L is the distance (cm) between two electrodes, R is the impedance (Ω) of the membrane, and S is the surface area (cm^2) of the electrodes.

Permeability

An H-cell setup was used for the permeability measurement of Fe(II) and Cr(III) ions. The left reservoir was filled with 1M Fe(II) ion solution ($FeCl_2{\cdot}4H_2O$) in 2M HCl, and the right reservoir was filled with 1M Cr(III) ion solution ($CrCl_3{\cdot}6H_2O$) in 2M HCl. The geometrical area of the exposed membrane was 1.77 cm^2 and the volume of the solution for each reservoir was 25 mL. Crossover contamination was measured by ultraviolet-visible spectrometry (UV-vis) on samples of solution which were taken from each reservoir at different time intervals. Samples were analyzed for Fe(II) concentration in right reservoir of Cr(III) solution, and for Cr(III) concentration in left reservoir of Fe(II) solution. Measured absorbance of samples from H-cell was converted into concentration based on standard absorbance-concentration curves. The permeability was calculated with following equation:

$$V_B \frac{dc_B(t)}{dt} = A\frac{P}{L}(c_A - c_B(t))$$

Here, c_A is the ion concentration in the original reservoir, and $c_B(t)$ is the time-dependent concentration of ion in the other reservoir which went through the membrane. V_B is the volume of one reservoir, A and L are the area and thickness of the membrane, and P is the permeability of ion. P is assumed to be independent of concentration. The permeability coating layer was calculated based on the data of h-DNf/oxide and c-DNf/oxide using the following equation:

$$\frac{L_A + L_B}{P_{A+B}} = \frac{L_A}{P_A} + \frac{L_B}{P_B}$$

A represents the c-DNf/oxide, B is the dense top oxide layer and A+B is the h-DNf/oxide.

An empirical figure of merit (β) is defined in the form of β = σ/P to demonstrate the ratio between the diffusivities of the desired ion and undesired ion in the membrane, i.e., the ratio of proton conductivity (σ) to Fe(II) permeability.

Flow battery test

A flow battery hardware was designed and fabricated in house. A picture of the device is shown in Fig. S8. Activated by 3:1 sulfuric acid and nitrate acid for 6 hours at 50 °C, two pieces of 0.6 cm thick graphite felt (AvCarb G200) were used as electrodes. Viton® fluoroelastomer rubber gaskets were used to seal the hardware. The active area of membrane was 1*1 cm^2. Densified and resin-filled impervious graphite plates (Graphtek FC-GR347B) served as current collects, which were sandwiched between copper end plates. The catholyte was prepared by dissolving 1 M $FeCl_2$ in 2 M HCl solution while the anolyte was 1 M $CrCl_3$ in 2 M HCl solution with 0.01 M Bi^{3+}. 8.5 ml catholyte and anolyte were circulated at a flow rate of 5 ml min^{-1} by a two-channel peristaltic pump (EW-77921-75, Cole-Parmer). All flow battery tests were performed at room temperature (25 °C). The galvanostatic charge and discharge experiments were conducted at 20 mA cm^{-2} with cut-off voltages between 0.7 and 1.2 V. Bismuth, serving as a catalyst for the anodic reaction, was plated onto the anode at 20 mA cm^{-2} before the initial charging.[51]

Results and Discussion

Fig. 1 shows the fabrication steps for the hierarchical membrane structure. Hydrated Nafion membrane is coated with a thin polydopamine layer (DNf) to improve the hydrophilicity of the surface. DNf is then filled with tungsten oxide in its hydrophilic ionic cluster regions, resulting in a composite structure (referred to as c-DNf/oxide). A dense tungsten oxide film is then coated on c-DNf/oxide to form the final membrane (denoted as h-DNf/oxide).

In order to realize the hierarchical structure, strong adhesion at the interface between the oxide coating and Nafion is essential. However, Nafion has a hydrophobic surface due to the perfluoroalkane backbone structure. To enable tungstic acid aqueous solution to wet Nafion surface, surface modification is required to render it hydrophilic. Inspiration is drawn from biological systems such as mussels that adhere to rocks through the use of dopamine.[52,53] Dopamine monomers are readily oxidized in air under basic pH conditions at room temperature to self-polymerize.[42,54] The polydopamine layer adheres strongly to almost any material, including PTFE and other anti-fouling materials.[52] Here, we utilize polydopamine as the adhesive layer to enhance the interaction between Nafion membrane and tungsten oxide coating layer and its hydrophilicity to facilitate the coating process. The polydopamine layer formed on Nafion is presumably very thin (~10 nm based on literature)[50] and could not be observed in cross section SEM images (Fig. S2(a)). A successful coating process was confirmed visually as the clear, transparent Nafion membrane became brown and semi-transparent (Fig. S1), as well as by a change in surface wetting properties. The contact angle of Nafion membrane decreased from 89° to 61° after polydopamine coating (Fig. S3).

Tungstic acid, which becomes tungsten oxide at elevated temperature or low pH, is the precursor to both c- and h-DNf/oxide structures. The acid is synthesized at around 25 °C through the reaction of tungsten powder with hydrogen peroxide. Nano-sized particles form as the aging progresses, and then serve as nucleation sites during the transformation from tungstic acid to tungsten oxide to enhance the coating layer formation.

A c-DNf/oxide structure is achieved by filling the ionic channels and clusters with the oxide precursor. Due to the small sizes of ionic clusters (~5 nm) in Nafion,[55] soaking the dry membrane directly is ineffective and so an infiltration method is used. The membrane is first soaked in methanol, causing it to swell, then the methanol is exchanged when soaking in the precursor solution. While there is no noticeable change in color of the membrane after the exchange with tungstic acid solution, the membrane becomes opaque and dark brown after a curing process, during which the precursor tungstic acid transfers into solid tungsten oxide. This indicates the successful filling of tungsten oxide into polymer membrane matrix (Fig. S1). Repeated solvent exchange and curing further increases the oxide loading amount in the Nafion with infiltrated tungsten oxide (c-DNf/oxide).

h-DNf/oxide was prepared by a simple dip coating method followed by a curing process. As a result of the enhanced hydrophilicity due to the polydopamine coating, the surface of DNf is readily wetted when dipped in a tungstic acid solution. The solution forms a uniform thin liquid layer covering the whole surface when the membrane is pulled out of the solution. During the curing process, elevated temperature promotes the solidification of precursor solution layer while the humidity keeps the membrane hydrated to avoid shrinkage and possible crack or delamination of the surface oxide layer due to mismatch in size changes between Nafion and the oxide. Smooth and uniform dark brown layers are coated on the membrane after repeated coating and curing (Fig. S6(b)). The quality of the coating was confirmed by SEM; the film is uniform and crack-free (Fig. 2(a)(b)). At a very high magnification, the coating layer is found to be formed by the aggregation of small particles of 5-15 nm in size (Fig. S2(b)). Additionally, a membrane with a tungsten oxide layer only on the surface but not in the bulk (l-DNf/oxide) was prepared by directly coating of DNf to confirm the contribution of oxide in polymer to the stability of oxide on polymer (Fig. S6).

EDX mapping was conducted on the surface of the h-DNf/oxide (Fig. S4). Tungsten and oxygen are distributed homogenously in the coating layer. Cross section SEM images also clearly show the dense and uniform coating layer with a EDX mapping was conducted on the surface of the h-DNf/oxide (Fig. S4). Tungsten and oxygen are distributed homogenously in the coating layer. Cross section SEM images

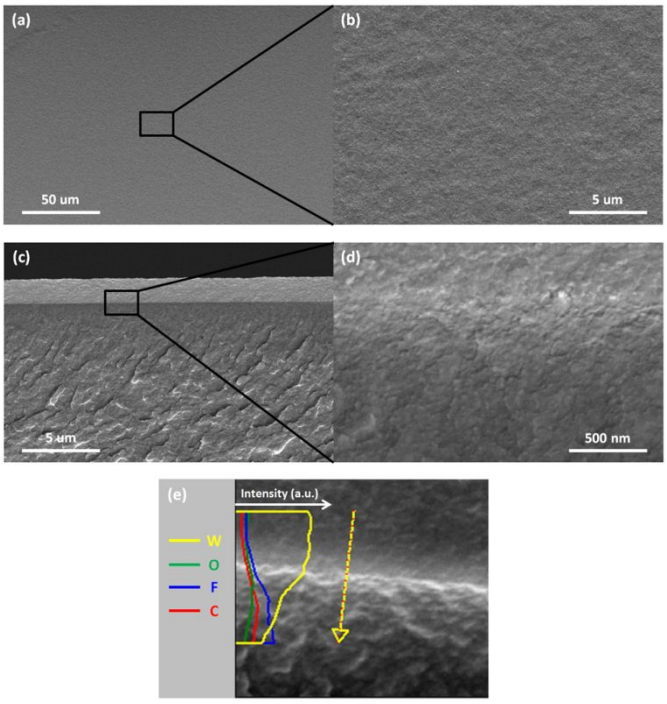

Fig. 2 SEM images of h-DNf/oxide: (a) (b) surface; (c) (d) cross section; (e) line scan EDX at the interface of tungsten oxide coating layer and Nafion membrane.

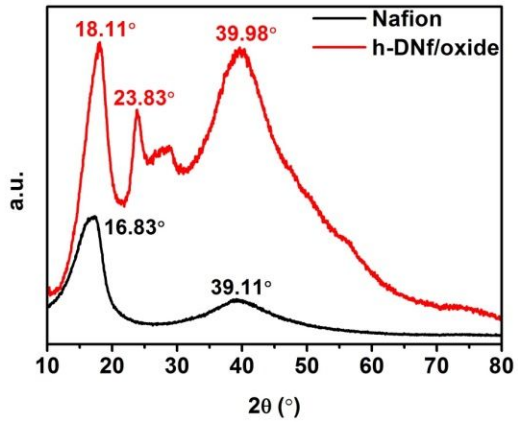

Fig. 3 XRD of Nafion and h-DNf/oxide.

also clearly show the dense and uniform coating layer with a thickness of 1.6 µm, confirming the structure is not porous even though it is formed from an aggregation of particles (Fig. 2(c)(d)). The interface between supporting Nafion membrane and coating layer is of exceptional quality with no visible voids and the boundary at the interface is not visible based on the high magnification SEM image (Fig. 2(d)). Line scan EDX shows a gradual compositional gradient across the interface, most noticeably for W (Fig. 2(e)). This observation confirms that our original design has been realized: the tungsten oxide phase is a continuous film on the surface but extends deeply into the Nafion structure. Such a structure is expected to contribute to a robust composite membrane. The good connection and adhesion could mitigate possible delamination at the interface, which is a critical problem for multilayered composite materials. EDX was also conducted on the cross section of h-DNf/oxide (Fig. S5). The low magnification EDX mapping shows the bulk polymer is mainly composed of carbon, oxygen, fluorine and sulfur. Surface coating layer contains concentrated tungsten and oxygen while tungsten is also uniformly distributed in bulk polymer matrix, further confirming the bilayer structure of oxide-in-polymer and oxide-on-polymer.

XRD was performed to investigate the structure of the membranes (Fig. 3). Shifting of Nafion peaks in h-DNf/oxide, from 16.83° and 39.11° to 18.11° and 39.98° respectively, indicates denser packing of polymer chains due to the interaction with tungsten oxide. The peak at 23.83° matches with several different types of tungsten oxide crystalline structure. As a result, the specific structure of filled tungsten oxide in Nafion cannot be determined based on XRD data. Further characterizations were performed to confirm the structure.

FTIR spectra were investigated to examine chemical structure of Nafion and h-DNf/oxide (Fig. 4(a)). Peaks at 1200, 1144 and 512 cm^{-1} are related to the C-F bonds on Nafion polymer backbone. C-O-C and C-S bonds on the side chain lead to twin peaks at 980, 968 cm^{-1} and a weak peak at 880 cm^{-1}

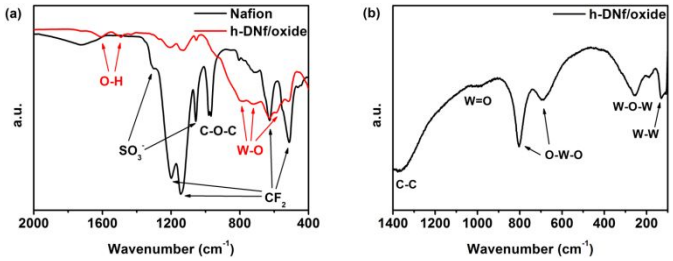

Fig. 4 Spectra of Nafion and h-DNf/oxide: (a) FT-IR; (b) Raman.

respectively. Shoulders at 1300 and 1144 cm^{-1} are assigned to the SO_3^- group. For the h-DNf/oxide, peaks in the range of 500-900 cm^{-1} are assigned to the W-O bond. Covered by the dense tungsten oxide coating layer, peaks from Nafion all decrease significantly. Raman spectroscopy was also performed on the h-DNf/oxide (Fig. 4(b)). C-C bond from Nafion polymer backbone exhibits a broad peak at 1370 cm^{-1}. Peaks observed at 1000, 690, 254 and 130 cm^{-1} correspond to W=O, O-W-O, W-O-W and W-W bonds, respectively. The peak at 800 cm^{-1}, also corresponding to the O-W-O bond, is associated with the monoclinic structure of tungsten oxide. It is thus concluded that tungsten oxide is successfully formed in the ionic clusters and its structure is likely monoclinic.

The thermal properties and compositions of membranes were investigated by TGA (Fig. 5). Both blank Nafion and h-DNf/oxide exhibit a three-stepped thermal degradation: loss of water during the first step before 270 °C; desulfonation of Nafion during the step around 350 °C; and decomposition of the Nafion polymer backbone during the last step above 400 °C. For both membranes, the first step is negligible as a result of pre-drying. After incorporating tungsten oxide into Nafion, the peaks of the second and third steps in derivative thermal gravimetric curves shifts from 363.9 °C and 448.9 °C to 377.0 °C and 469.5 °C, respectively (Fig. 5(b)). The enhanced thermal stability of h-DNf/oxide provides evidence for the interaction between oxide and polymer. The residual weight indicates that the tungsten oxide loading is 6.6%.

High mechanical stability of PEM is necessary for long-term practical operation of flow batteries. Nafion membrane in its dry state showed a Young's modulus of 142.5 MPa, a yield stress at 7.67 MPa with an 8.5% strain, and a failure stress at 25.9 MPa with a 223.3% strain (Fig. 6, Table S1). Nafion membrane becomes much weaker when hydrated, with a 35.5 MPa Young's modulus, 4.95 MPa yield stress and 20.4 MPa of failure stress. The yield strain increases by 2.6 times to 22%,

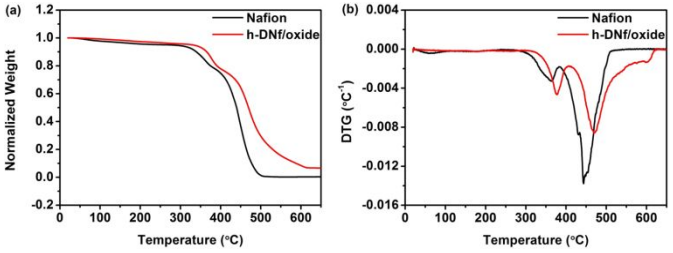

Fig. 5 Thermogravimetric analysis of Nafion and h-DNf/oxide: (a) TG; (b) DTG.

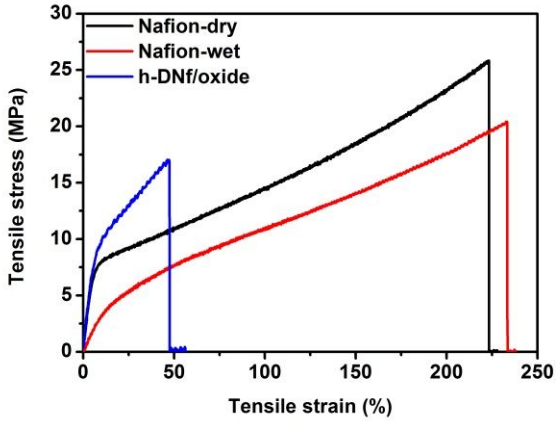

Fig. 6 Stress-strain curves of Nafion and h-DNf/oxide

yet the ultimate strain remains almost the same. A decrease in the Young's modulus and a change in the yield point after hydration are due to the high water uptake and swelling ratio of the Nafion membrane. High water content enables faster proton transportation but also increases polymer chain mobility, leading to poor mechanical stability. The h-DNf/oxide is significantly reinforced, reaching a Young's modulus of 148.7 MPa and a yield stress of 9.29% at an elongation of 9.1%, performances that are superior even when compared with the dry Nafion membrane. The ultimate strain is decreased significantly to only 47.3% without a large drop in the ultimate stress. The coated tungsten oxide layer on the polymer makes little contribution to the mechanical properties of bulk membrane due to the limited thickness. Tungsten oxide in the polymer likely changes the mechanical properties of the membrane in three aspects: (1) Interactions between tungsten oxide and polymer chains suppress chain mobility and increase chain packing density; (2) tungsten oxide filled in ionic clusters forms a continuous rigid oxide network across the polymer matrix serving as reinforced concrete to achieve outstanding mechanical stability; (3) tungsten oxide replaces the water in hydrated polymer which could also reduce chain mobility. The mechanical stability of the h-DNf/oxide is not only beneficial to cell operation but also helps prevent the failure of coating layer caused by mechanical deformation or dimensional variation due to humidity change.

Water uptake (WU) and swelling (SW) are important parameters for composite ion exchange membranes (Table 1). While high water uptake usually facilitates ion transport, the correspondingly high swelling might compromise the mechanical integrity of the composite structure, particularly for the oxide on polymer configuration. The DNf membrane exhibits a water uptake of 38.2% and a swelling of 44.1%, similar to baseline Nafion. Due to its very low thickness, the polydopamine coating layer has negligible influence on the water uptake and swelling of the bulk membrane.

Consequently, the significant reduction in swelling ratio is due to the incorporation of tungsten oxide. Most failures of composite membranes with layered structures, especially those formed by coating rigid inorganic materials on soft polymer supports, are caused by delamination or cracks due to different swelling ratios of the layers. Controlling the water uptake and swelling could effectively enhance the stability as well as mechanical properties of composite membrane. The tungsten oxide coating layer of l-DNf/oxide exhibits dramatic delamination after soaking in DI water for 24 hours, while h-DNf/oxide maintains its original structure after one week, confirming the contribution of infiltrated tungsten oxide on membrane stability (Fig. S6).

Table 1 Water uptake, area swelling and ion conductivity of Nafion and composite membranes.

	WU [%]	SW [%]	σ_{H^+} [a] [mS/cm]	σ_{H^+}/WU	σ_{K^+} [a] [mS/cm]	σ_{K^+}/WU
Nafion	38.9	46.6	54.1	1.39	8.0	0.21
DNf	38.2	44.1	4.6	0.12	-	-
h-DNf/oxide	12.1	16.9	22.8	1.88	4.6	0.38

All data measured at room temperature. [a] through plane, at 100% RH

Ionic conductivities (σ) were measured by a through-plane two-probe method at hydrated state (Table 1). The proton conductivity (σ_{H^+}) of DNf membrane is 4.6 mS/cm, only 8.5% of 54.1 mS/cm, the conductivity of Nafion. The dramatic conductivity drop caused by the additional layer with negligible thickness suggests the conductivity of polydopamine is very low. Interestingly, after introducing tungsten oxide, the conductivity of h-DNf/oxide increases to 22.8 mS/cm, which represents a manageable reduction from that of Nafion. Filling polydopamine with proton conductive tungsten oxide and rebuilding the proton transport pathway likely contributes to the recovery of conductivity. The ratio of conductivity over water uptake (σ/WU) is a metric that measures the effectiveness of water in promoting ion conduction. The σ_{H^+}/WU of h-DNf/oxide is 1.88 compared with 1.39 for baseline Nafion. Hence, tungsten oxide filling in the ion channels appears to help enhance the water facilitated proton conduction.

We also measured the potassium ion conductivity (σ_{K^+}) of Nafion and the composite (Table 1). For flow batteries such as Fe/Fe and Cr/Fe, KCl is often the supporting electrolyte and K^+ transports through the cell membrane. During ion exchange, we expect hydrated tungsten oxide to change to its potassium form. In this regard, hydrated potassium tungsten bronze is well known. However, K^+ conductivities in them have not been well studied. Our measurement produced a conductivity of 8.0 mS/cm for K^+ exchanged Nafion, or 14.8% of the proton conductivity. The h-DNf/oxide showed a K^+ conductivity of 4.6 mS/cm, or 20.2% of proton conductivity. The σ_{K^+}/WU value for the h-DNf/oxide reaches 0.38, in comparison, the value for Nafion is 0.21. The smaller difference in σ/WU for K^+ vs H^+ compared with Nafion, indicates that the h-DNf/oxide relies much less on water to transport ions.

Permeability of active species is another key parameter of CEM

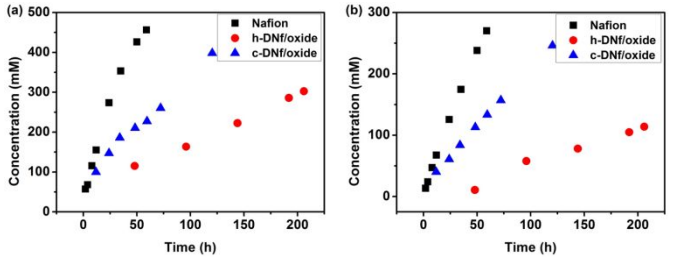

Fig. 7 Ion crossover tests of Nafion, c-DNf/oxide and h-DNf/oxide: (a) Fe(II); (b) Cr(III).

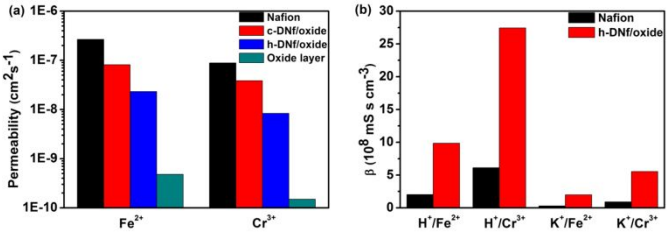

Fig. 8 Comparisons of (a) ion permeabilities and (b) β for Nafion and the composite membranes. β is defined as the ratio of conductivity to permeability.

for flow batteries. The permeabilities for Fe(II) and Cr(III) ions are measured simultaneously by filling two sides of an H-cell with solutions containing different ions. This represents the discharged state of a Fe/Cr flow battery. The crossover of Cr(III) ion can be visibly observed based on its dark green color while the crossover of Fe(II) ion could not be observed since its light green color is similar to that for the Cr(III) ion. The h-DNf/oxide shows much smaller crossover for both Fe(II) and Cr(III) ion, compared with baseline Nafion. Fig. 7(a) and (b) show test results for both ions when using three different membranes: baseline Nafion, h-DNf/oxide, and c-DNf/oxide. The Fe(II) ion crossover rate of Nafion is the highest and after 50 hours, starts to decrease as the solution reaches the concentration equilibrium. As shown in Fig. 8(a), for both Fe(II) and Cr(III) ions, h-DNf/oxide still maintains a constant low crossover rate after 210 hours, suggesting the stability of coating layer is not compromised over extended testing. For h-DNf/oxide, the permeability of Fe(II) and Cr(III) ions are decreased by an order of magnitude, from 2.66×10^{-7} cm^2 s^{-1} and 8.84×10^{-8} cm^2 s^{-1} to 2.31×10^{-8} cm^2 s^{-1} and 8.34×10^{-9} cm^2 s^{-1} respectively. Cr(III) ion exhibits lower permeability for both baseline and h-DNf/oxide due to its higher valence state. c-DNf/oxide also exhibits some capability to decrease the metal ion crossover, which are measured to be 8.14×10^{-8} cm^2 s^{-1} and 3.85×10^{-8} cm^2 s^{-1} for Fe(II) and Cr(III) ions respectively. The permeability difference between membranes of h-DNf/oxide and c-DNf/oxide can be attributed to the dense surface tungsten oxide layer. Considering the thickness of Nafion membrane and coating layer, the dense tungsten oxide coated layer shows extraordinarily low permeability: 4.88×10^{-10} cm^2 s^{-1} for Fe(II) ion, 0.18% of baseline Nafion and 1.94% of c-DNf/oxide; 1.48×10^{-10} cm^2 s^{-1} for Cr(III) ion, 0.17% of bare Nafion and 1.77% of c-DNf/oxide. An empirical figure of merit (β) is defined as the ratio of conductivity to permeability to demonstrate the ratio between the diffusivities of the desired ion and undesired ion in the membrane. In Fig. 8(b), h-DNf/oxide shows increased β of H^+ and K^+ over Fe^{2+} and Cr^{3+}. The H^+/Cr^{3+} β of h-DNf/oxide reaches 2.74×10^9 mS s cm^{-3}. Therefore, the hierarchical composite structures greatly enhance the selectivity of membrane.

The flow battery performances of membranes were evaluated in a lab-scale single cell iron-chromium flow battery (Fig. S8) as a proof of concept. For the galvanostatic charge and discharge experiments, relatively high capacity to active membrane area was utilized to emphasize the effect of crossover by prolonging the time of each cycle (Fig. 9). Although only limited number of cycles were performed, the total duration of tests was actually similar to those commonly reported in the literature.[56-58] At a current density of 20 mA cm^{-2}, the flow battery assembled with Nafion as the separator exhibited a quick and dramatic discharge capacity decay, retaining only 29.5 mAh after 42.2 hours from a first cycle capacity of 106.6 mAh. The dark color of catholyte after cycling indicated the high rate of irreversible crossover which led to the rapidly decreasing capacity (Fig. S9). Benefiting from the much decreased crossover rate due to the hierarchical composite structure, the capacity decay was mitigated by the dense oxide layer of h-DNf/oxide layer (Fig. S11). The flow battery with h-DNf/oxide delivered a capacity of 87.9 mAh after 47.9 hours, which is about 3 times of Nafion. The color change of catholyte was also very minor. Compared with Nafion, even without the dense surface oxide layer, c-DNf/oxide still showed obvious improvement, which maintained a discharge capacity of 55.4 mAh. As shown in the Fig. 9(b), due to the severe crossover, the flow battery with Nafion exhibited a much larger overpotential than those with either h-DNf/oxide or c-DNf/oxide. We should note that the columbic efficiencies, a commonly used performance metric, for all three batteries are very similar at about 85% despite the large difference in capacity retention. This indicates that crossover in this case reduced the reversible capacity of the batteries while the coulomb efficiency was determined by other processes such as hydrogen evolution.[4] In summary, the overall trend of flow battery performance is consistent with the permeability and selectivity results from static H-cell tests. With no obvious influence from the minor decrease in conductivity, the hierarchical composite structure can greatly mitigate the crossover of active species which represents an important progress in addressing the well known trade-off between conductivity and selectivity for flow battery membranes.

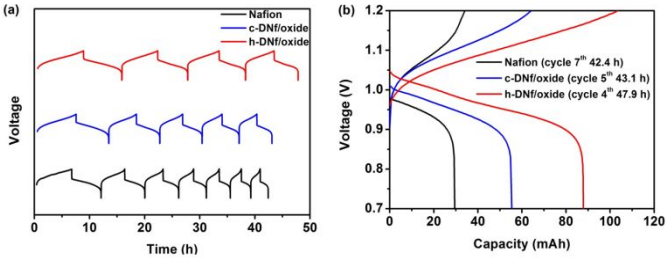

Fig. 9 Charge-discharge profile of Nafion and composite membranes at 20 mA cm^{-2}: (a) cycling, (b) comparison after similar cycling time.

Conclusions

A hierarchical composite ion exchange membrane has been developed by integrating Nafion and tungsten oxide. Proton conducting tungsten oxide is infiltrated into ionic clusters of Nafion membrane to reduce water uptake, swelling ratio and enhance stability while maintaining reasonable conductivity. A dense, crack-free tungsten oxide layer is coated on the surface to reduce the permeability of active species. A stable oxide-on-polymer structure is enabled by the dimensionally stable oxide-in-polymer composite structure. An order of magnitude decrease of permeability of Fe(II) and Cr(III) ions is observed for the hierarchical composite membrane while maintaining comparable conductivity. The dense oxide coating layer shows three orders of magnitude lower permeability than Nafion. Such composite membrane with a hierarchical structure provides a strategy to solve the trade-off between conductivity and permeability of ion exchange membranes. The positive effect of reduced crossover is confirmed in a small lab-scale iron-chromium flow battery with improved capacity retention with cycling and time. Further work is needed to scale up the flow battery and optimize its design to fully realize the benefit of the composite membrane. Nevertheless, our method of fabricating stable bilayer inorganic-polymer structure has the potential to be applied to many different ion conductors that underpin energy conversion and storage devices.

Conflicts of interest

There are no conflicts to declare.

Acknowledgements

We thank the University of California, San Diego for financial support. This work was performed in part at the San Diego Nanotechnology Infrastructure (SDNI) of UCSD, a member of the National Nanotechnology Coordinated Infrastructure, which is supported by the National Science Foundation (Grant ECCS-1542148).

Notes and references

1 D. Larcher and J. M. Tarascon, *Nat. Chem.*, 2014, **7**, 19-29.
2 Z. Yang, J. Zhang, M. C. W. Kintner-Meyer, X. Lu, D. Choi, J. P. Lemmon and J. Liu, *Chem. Rev.*, 2011, **111**, 3577-3613.
3 G. L. Soloveichik, *Chem. Rev.*, 2015, **115**, 11533-11558.
4 W. Wang, Q. Luo, B. Li, X. Wei, L. Li and Z. Yang, *Adv. Funct. Mater.*, 2012, **23**, 970-986.
5 P. Leung, X. Li, C. Ponce de Leon, L. Berlouis, C. T. J. Low and F. C. Walsh, *RSC Adv.*, 2012, **2**, 10125-10156.
6 C. Ding, H. Zhang, X. Li, T. Liu and F. Xing, *J. Phys. Chem. Lett.*, 2013, **4**, 1281-1294.
7 A. Parasuraman, T. M. Lim, C. Menictas and M. Skyllas-Kazacos, *Electrochim. Acta*, 2013, **101**, 27-40.
8 G. Kear, A. Shah Akeel and C. Walsh Frank, *Int. J. Energy Res.*, 2011, **36**, 1105-1120.
9 A. Z. Weber, M. M. Mench, J. P. Meyers, P. N. Ross, J. T. Gostick and Q. Liu, *J. Appl. Electrochem.*, 2011, **41**, 1137-116.
10 X. Li, H. Zhang, Z. Mai, H. Zhang and I. Vankelecom, *Energy Environ. Sci.*, 2011, **4**, 1147-1160.
11 M. Skyllas-Kazacos, M. H. Chakrabarti, S. A. Hajimolana, F. S. Mjalli and M. Saleem, *J. Electrochem. Soc.*, 2011, **158**, R55-R79.
12 B. Dunn, H. Kamath and J.-M. Tarascon, *Science*, 2011, **334**, 928-935.
13 C. Ponce de León, A. Frías-Ferrer, J. González-García, D. A. Szánto and F. C. Walsh, *J. Power Sources*, 2006, **160**, 716-732.
14 B. Schwenzer, J. Zhang, S. Kim, L. Li, J. Liu and Z. Yang, *ChemSusChem*, 2011, **4**, 1388-1406.
15 H. Prifti, A. Parasuraman, S. Winardi, T. M. Lim and M. Skyllas-Kazacos, *Membranes*, 2012, **2**, 275-306.
16 H. Strathmann, A. Grabowski and G. Eigenberger, *Ind. Eng. Chem. Res.*, 2013, **52**, 10364-10379.
17 X. L. Zhou, T. S. Zhao, L. An, Y. K. Zeng and L. Wei, *J. Power Sources*, 2017, **339**, 1-12.
18 F. Cheng, J. Liang, Z. Tao and J. Chen, *Adv. Mater.*, 2011, **23**, 1695-1715.
19 J. Liu, J. G. Zhang, Z. Yang, J. P. Lemmon, C. Imhoff, G. L. Graff, L. Li, J. Hu, C. Wang, J. Xiao, G. Xia, V. V. Viswanathan, S. Baskaran, V. Sprenkle, X. Li, Y. Shao and B. Schwenzer, *Adv. Funct. Mater.*, 2013, **23**, 929-946.
20 Y. Li, G. He, S. Wang, S. Yu, F. Pan, H. Wu and Z. Jiang, *J. Mater. Chem.* A, 2013, **1**, 10058-10077.
21 C.-H. Lin, M.-C. Yang and H.-J. Wei, *J. Power Sources*, 2015, **282**, 562-571.
22 J. Zhang, G. Wang, F. Wang, J. Zhang, J. Chen and R. Wang, *J. Electroanal. Chem.*, 2016, **783**, 76-81.
23 B. Yin, L. Yu, B. Jiang, L. Wang and J. Xi, *J. Solid State Electrochem.*, 2016, **20**, 1271-1283.
24 N. Wang, S. Peng, H. Wang, Y. Li, S. Liu and Y. Liu, *Electrochem. Commun.*, 2012, **17**, 30-33.
25 C. Jia, Y. Cheng, X. Ling, G. Wei, J. Liu and C. Yan, *Electrochim. Acta*, 2015, **153**, 44-48.
26 M. A. Aziz and S. Shanmugam, *J. Power Sources*, 2017, **337**, 36-44.
27 Y. Liu, J. Wang, H. Zhang, C. Ma, J. Liu, S. Cao and X. Zhang, *J. Power Sources*, 2014, **269**, 898-911.
28 L. Yu, F. Lin, L. Xu and J. Xi, *RSC Adv.*, 2016, **6**, 3756-3763.
29 L. Su, D. Zhang, S. Peng, X. Wu, Y. Luo and G. He, *Int. J. Hydrogen Energy*, 2017, **42**, 21806-21816.
30 P. S. Goh, A. F. Ismail, S. M. Sanip, B. C. Ng and M. Aziz, *Sep. Purif. Technol.*, 2011, **81**, 243-264.
31 S. Liu, X. Sang, L. Wang, J. Zhang, J. Song and B. Han, *Electrochim. Acta*, 2017, **257**, 243-249.
32 J. Wang, X. Yue, Z. Zhang, Z. Yang, Y. Li, H. Zhang, X. Yang, H. Wu and Z. Jiang, *Adv. Funct. Mater.*, 2012, **22**, 4539-4546.
33 J. Wang, Z. Zhang, X. Yue, L. Nie, G. He, H. Wu and Z. Jiang, *J. Mater. Chem. A*, 2013, **1**, 2267-2277.
34 M. L. Di Vona, Z. Ahmed, S. Bellitto, A. Lenci, E. Traversa and S. Licoccia, *J. Membr. Sci.*, 2007, **296**, 156-161.
35 Y. Yin, T. Xu, G. He, Z. Jiang and H. Wu, *J. Power Sources*, 2015, **276**, 271-278.
36 J. Xi, Z. Wu, X. Qiu and L. Chen, *J. Power Sources*, 2007, **166**, 531-536.
37 X. Teng, Y. Zhao, J. Xi, Z. Wu, X. Qiu and L. Chen, *J. Membr. Sci.*, 2009, **341**, 149-154.
38 B. P. Tripathi and V. K. Shahi, *Prog. Polym. Sci.*, 2011, **36**, 945-979.
39 L. C. Klein, Y. Daiko, M. Aparicio and F. Damay, *Polymer*, 2005, **46**, 4504-4509.
40 Z. Chen, B. Holmberg, W. Li, X. Wang, W. Deng, R. Munoz and Y. Yan, *Chem. Mater.*, 2006, **18**, 5669-5675.
41 Q. Luo, H. Zhang, J. Chen, P. Qian and Y. Zhai, *J. Membr. Sci.*, 2008, **311**, 98-103.
42 F. Pan, H. Jia, S. Qiao, Z. Jiang, J. Wang, B. Wang and Y. Zhong, *J. Membr. Sci.*, 2009, **341**, 279-285.
43 S. Zhong, X. Cui, T. Fu and H. Na, *J. Power Sources*, 2008, **180**, 23-28.

44 Y. Zhao, K. Tang, H. Liu, B. Van der Bruggen, A. Sotto Díaz, J. Shen and C. Gao, *J. Membr. Sci.*, 2016, **520**, 262-271.
45 M. Hibino, H. Nakajima, T. Kudo and N. Mizuno, *Solid State Ionics*, 1997, **100**, 211-216.
46 Y. M. Li, M. Hibino, M. Miyayania and T. Kudo, *Solid State Ionics*, 2000, **134**, 271-279.
47 Y. Tanaka, M. Miyayama, M. Hibino and T. Kudo, *Solid State Ionics*, 2004, **171**, 33-39.
48 Y. Li, M. Hibino, M. Miyayania and T. Kudo, *Solid State Ion.*, 2000, **134**, 271-279.
49 P. Kumar and S. Yashonath, *J. Chem. Sci.*, 2006, **118**, 135-154.
50 J. Wang, L. Xiao, Y. Zhao, H. Wu, Z. Jiang and W. Hou, *J. Power Sources*, 2009, **192**, 336-343.
51 C. D. Wu, D. A. Scherson, E. J. Calvo, E. B. Yeager and M. A. Reid, *J. Electrochem. Soc.*, 1986, **133**, 2109-2112.
52 H. Lee, S. M. Dellatore, W. M. Miller and P. B. Messersmith, *Science*, 2007, **318**, 426-430.
53 H. Lee, Y. Lee, A. R. Statz, J. Rho, T. G. Park and P. B. Messersmith, *Adv. Mater.*, 2008, **20**, 1619-1623.
54 M. Xiao, Y. Li, M. C. Allen, D. D. Deheyn, X. Yue, J. Zhao, N. C. Gianneschi, M. D. Shawkey and A. Dhinojwala, *ACS Nano*, 2015, **9**, 5454-5460.
55 J. Y. Li and S. Nemat-Nasser, *Mech. Mater.*, 2000, **32**, 303-314.
56 Y. Zeng, X. Zhou, L. An, L. Wei, T. Zhao, *J. Power Sources*, 2016, **324**, 738-744.
57 Y. Zeng, T. Zhao, L. An, *J. Power Sources*, 2015, **300**, 438-443.
58 H. Zhang, Y. Tian, J. Li, B. Xue, *Electrochim. Acta*, 2017, **248**, 603-613.

A hierarchically structured composite ion exchange membrane is developed to solve the trade-off between conductivity and selectivity.